A Modified Space-Time Conservation Element and Solution Element Method for Euler and Navier-Stokes Equations

Zeng-Chan Zhang[1] and S.T. John Yu[2]
Mechanical Engineering Department
Wayne State University, Detroit, MI 48202

Sin-Chung Chang[3]
NASA Glenn Research Center
Cleveland, OH 44135

Ananda Himansu[4]
Taitech Inc.,
NASA Glenn Research Center
Cleveland, OH 44135

Philip C.E. Jorgenson[5]
NASA Glenn Research Center
Cleveland, OH 44135

Abstract

In this paper, we report a variation of Chang's Space-Time Conservation Element and Solution Element CE/SE Method for structured mesh. The algorithm of the present modified CE/SE method is even simpler than the original CE/SE method. Nevertheless, all advantageous features of the original CE/SE method have been retained, including a unified treatment of space and time, accurate calculation of the space-time flux, high-fidelity resolution of unsteady flow motions, and full compliance with the physics of initial valued problems. The present modified method is also extended to solve Navier Stokes equations. To calculate the viscous flux terms, a 'midpoint rule' is used. In the setting of space-time flux conservation, two boundary-condition treatments for solid wall are introduced. Numerical results show that the present Navier Stokes solver can be used for high-speed flows as well as low-Mach-number flows without preconditioning. Results of several standard flow problems show that the present method is efficient and accurate.

1 Introduction

The Space-Time Conservation Element and Solution Element Method (or the CE/SE Method for short), originally proposed by Chang [1], is a new numerical framework for conservation laws. The CE/SE method has many non-traditional features, including a unified treatment of space and time, the introduction of conservation element (CE) and solution element (SE), and a novel shock capturing strategy without Rieman solver. More than all, the CE/SE method is a genuine multidimensional scheme because the method has been constructed without dimensional splitting. Thus, calculations of multidimensional equations and source terms are more realistic. To date, numerous highly accurate solutions have been obtained, including traveling and interacting shocks, acoustic waves, shedding vortices, detonation waves, shock/acoustic waves interaction, shock/vortex interaction, and cavitating flows.

In the original CE/SE method, the flow variable U and its spatial gradient U_x are considered as unknowns and that are solved simultaneously. Therefore, for equations in one spatial dimension, two CEs at each grid point are constructed to derive two discrete equations for U and U_x. Similarly, three and four CEs at each grid point are needed in two and three-dimensional cases, respectively.

In this paper, the original CE/SE method is modified such that only one CE at each grid point is employed for equations in one, two and three spatial dimensions. As will be illustrated in the following sections, the definitions of the modified CE are very simple. Accordingly, the logic of the modified CE/SE scheme is simple and can be easily implemented.

As compared to the original CE/SE method, CE in the present method is used to calculate U only; U_x is calculated by a central difference method . For equations in one spatial dimension, the modified scheme is a special case of Chang's a-ε scheme. For equations in two and three dimensions, this new modified method can be easily applied to structured meshes. As such, it can serve as an alternative solver for time-accurate solutions in well-established CFD codes. The rest of the paper is organized as follows.

In Section 2, the modified CE/SE method for two-dimensional Euler equations will be

---

[1] Visiting Professor from Tsinghua University, China, Email: zz9@nova.eng.wayne.edu
[2] Associate Professor, AIAA Member, Email: styu@eng.wayne.edu
[3] Senior Aerospace Engineer, Email: sin-chung,chang@lerc.nasa.gov
[4] Senior Scientist, Email: fshiman@trout.lerc.nasa.gov
[5] Senior Aerospace Engineer, Email:aejorgen@lerc.nasa.gov

illustrated. Two definitions of CE and SE will be presented. In section 3, the modified CE/SE scheme is extended to solve the Navier-Stokes equations. A 'midpoint rule' is used to integrate the viscous fluxes as part of the space-time flux conservation. In section 4, we discuss two numerical treatments for wall boundary based on the concept of space-time flux conservation. The first one is similar to traditional wall boundary treatment. The second one is designed based on a novel pseudo-reflection concept, which proves to be more accurate and numerically more stable. In section 5, several prototype flow problems are calculated using the modified CE/SE scheme. The results are verified by comparing with experimental data or previously reported numerical solutions. We then offer concluding remarks and give cited references.

2. The Modified CE/SE Method for Two-Dimensional Euler Equations

Consider the two-dimensional unsteady Euler equations of a perfect gas:

$$\partial U_m / \partial t + \partial F_m / \partial x + \partial G_m / \partial y = 0 ,$$
$$m=1,2,3,4 \qquad (2.1)$$

Let $x_1=x$, $x_2=y$ and $x_3=t$ be the coordinates of the three-dimensional Euclidean space E_3. Assuming smoothness of the physical solutions, Eq.(2.1) is equivalent to the integral equation:

$$\oint_{S(V)} H_m \cdot ds = 0 , \qquad m=1,2,3,4 \qquad (2.2)$$

Here $S(V)$ is the boundary of an arbitrary space-time region V in E_3, and $H_m=(F_m, G_m, U_m)$.

A CE in the CE/SE method is a space-time region, in which the space-time flux conservation, Eq. (2.2), is enforced. A SE is a different space-time region, in which the flow variables are supposed to be smooth and Eq. (2.1) is valid. Since the flow variables are smooth inside a SE, discretization of the flow variables with a prescribed order of accuracy can be performed. In the CE/SE method, the first order Taylor series expansion is used. In what follows, two kinds of CEs and SEs are illustrated for the present modified method.

2.1 CE and SE of the First Kind

In Fig. 1(a), representative grid points in a *x-y* plane are depicted. There are two groups of grid points, marked by open circles and crosses, which represent mesh nodes at two different time levels. One CE and one SE are associated with a mesh point *(i , j, n)*. Here the CE is the quadrilateral cylinder EFGHE'F'G'H', and the SE is a union of the

quadrilateral cylinder P"Q"R'S"P'Q'R'S' and the horizontal plane EFGH. Refer to Fig. 1(b).
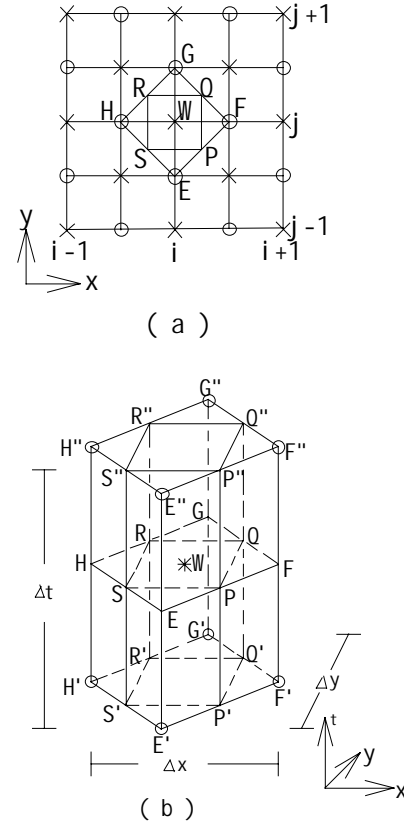

(a)

(b)

Fig.1 The representative grid points in x-y plane and the definitions of CE and SE.

To proceed, for any *(x, y, t)* ∈ SE *(i, j, n)*, $U_m(x, y, t)$, $F_m(x, y, t)$ and $G_m(x, y, t)$ are approximated by the first-order Taylor expansion:

$$U_m^*(x, y, t; i, j, n) = (U_m)_{i,j}^n + (U_{mx})_{i,j}^n (x - x_i)$$
$$+ (U_{my})_{i,j}^n (y - y_j) + (U_{mt})_{i,j}^n (t - t^n)$$
$$(2.3a)$$

$$F_m^*(x, y, t; i, j, n) = (F_m)_{i,j}^n + (F_{mx})_{i,j}^n (x - x_i)$$
$$+ (F_{my})_{i,j}^n (y - y_j) + (F_{mt})_{i,j}^n (t - t^n)$$
$$(2.3b)$$

$$G_m^*(x, y, t; i, j, n) = (G_m)_{i,j}^n + (G_{mx})_{i,j}^n (x - x_i)$$
$$+ (G_{my})_{i,j}^n (y - y_j) + (G_{mt})_{i,j}^n (t - t^n)$$
$$(2.3c)$$

Accordingly,

$$H_m^*(x, y, t; i, j, n) = (F_m^*(x, y, t; i, j, n),$$
$$, G_m^*(x, y, t; i, j, n), U_m^*(x, y, t; i, j, n)) \quad (2.4)$$

Thus Eq. (2.2) can be approximated by its discrete counterpart:

$$\oint_{S(CE(i,j,n))} H_m *\cdot ds = 0, \qquad (2.5)$$

Substituting Eq. (2.3) into Eq. (2.1), one gets

$$(U_{mt})_{i,j}^n = -(F_{mx})_{i,j}^n - (G_{my})_{i,j}^n \qquad (2.6)$$

Therefore, in two-dimensional case, the independent discrete variables at each grid point are U_m, U_{mx} and U_{my}. By substituting Eqs. (2.3) and (2.4) into Eq.(2.5), we obtain:

$$(U_m)_{i,j}^n =$$

$$\left\{Q_m^{(1)}(-\Delta x/2)\right\}_{i-1/2,j}^{n-1/2} + \left\{Q_m^{(1)}(\Delta x/2)\right\}_{i+1/2,j}^{n-1/2}$$

$$+ \left\{Q_m^{(2)}(\Delta y/2)\right\}_{i,j+1/2}^{n-1/2} + \left\{Q_m^{(2)}(-\Delta y/2)\right\}_{i,j-1/2}^{n-1/2}$$

$$(2.7)$$

Where

$$Q_m^{(1)}(\Delta x) = \{(2U_m - \Delta x \cdot U_{mx}) - \Delta t/2 \cdot [G_{my} +$$
$$(4F_m - \Delta x \cdot F_{mx} + \Delta t \cdot F_{mt})/\Delta x]\}/8$$

$$Q_m^{(2)}(\Delta y) = \{(2U_m - \Delta y \cdot U_{my}) - \Delta t/2 \cdot [F_{mx} +$$
$$(4G_m - \Delta y \cdot G_{my} + \Delta t \cdot G_{mt})/\Delta y]\}/8$$

Equation (2.7) is the discrete equation for the numerical solution of U_m.

To solve U_{mx} and U_{my}, numerical continuity of U_m* at the common grid points E, F, G and H between neighboring SEs are assumed. Refer to Fig. 2(b). This lead to the central difference equation for U_{mx} and U_{my}:

$$(U_{mx})_{i,j}^n = [(U_{mx}^+)_{i,j}^n + (U_{mx}^-)_{i,j}^n]/2, \qquad (2.8a)$$

$$(U_{my})_{i,j}^n = [(U_{my}^+)_{i,j}^n + (U_{my}^-)_{i,j}^n]/2, \qquad (2.8b)$$

Where

$$(U_{mx}^\pm)_{i,j}^n = \pm[(U_m')_{i\pm1/2,j}^n - (U_m)_{i,j}^n]/(\Delta x/2)$$

$$(U_{my}^\pm)_{i,j}^n = \pm[(U_m')_{i,j\pm1/2}^n - (U_m)_{i,j}^n]/(\Delta y/2)$$

$$(U_m')_{i\pm1/2,j}^n = \left\{U_m + \Delta t \cdot U_{mt}/2\right\}_{i\pm1/2,j}^{n-1/2}$$

$$(U_m')_{i,j\pm1/2}^n = \left\{U_m + \Delta t \cdot U_{mt}/2\right\}_{i,j\pm1/2}^{n-1/2}$$

For flows with discontinuities such as shocks, Eq. (2.8) can be further modified by a re-weighting procedure:

$$(U_{mx})_{i,j}^n = W((U_{mx}^-)_{i,j}^n,(U_{mx}^+)_{i,j}^n,\alpha) \qquad (2.9a)$$

$$(U_{my})_{i,j}^n = W((U_{my}^-)_{i,j}^n,(U_{my}^+)_{i,j}^n,\alpha) \qquad (2.9b)$$

Where the re-weighting function W is defined by

$$W(x_-,x_+,\alpha) = \frac{|x_+|^\alpha x_- + |x_-|^\alpha x_+}{|x_+|^\alpha + |x_-|^\alpha}$$

Here α is an adjustable constant, usually $\alpha=1$ or 2. Other limiters could also be used, e.g., the minmod function:

$$(U_{mx})_{i,j}^n = \text{minmod}\{(U_{mx}^-)_{i,j}^n,(U_{mx}^+)_{i,j}^n\} \qquad (2.10a)$$

$$(U_{my})_{i,j}^n = \text{minmod}\{(U_{my}^-)_{i,j}^n,(U_{my}^+)_{i,j}^n\} \qquad (2.10b)$$

Equations (2.7) and (2.8) (or (2.9) or (2.10)) are the modified CE/SE scheme for solving the 2-D Euler equations based on the CE and SE of the first kind.

2.2 CE and SE of the Second Kind

The representative grid points in x-y plane and the definition of CE and SE are depicted in Fig.2. For each mesh point (i, j, n), there is one CE and one SE. Here the CE is defined as a quadrilateral cylinder ABCDA'B'C'D'. The SE is the union of the quadrilateral cylinder EFGHE'F'G'H' and the horizontal plane ABCD. Refer to Fig. 2(b). The second definition of CE and SE here can be obtained by performing a coordinate transformation of 45° on the CE and SE of the first kind.
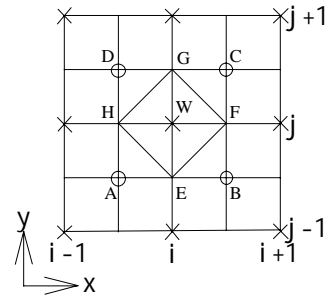
(a)
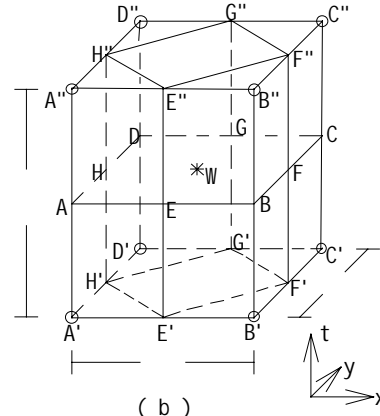
(b)

Fig. 2 Representative grid points and the definitions of SE and CE of the second kind.

Following the same procedure in the previous section, we can obtain the discrete equation for U_m,

$$(U_m)_{i,j}^n = \{Q_m(-\Delta x/2, \Delta y/2)\}_{i-1/2, j+1/2}^{n-1/2}$$
$$+ \{Q_m(-\Delta x/2, -\Delta y/2)\}_{i-1/2, j-1/2}^{n-1/2}$$
$$+ \{Q_m(\Delta x/2, -\Delta y/2)\}_{i+1/2, j-1/2}^{n-1/2}$$
$$+ \{Q_m(\Delta x/2, \Delta y/2)\}_{i+1/2, j+1/2}^{n-1/2} \quad (2.11)$$

Where
$$Q_m(\Delta x, \Delta y) = (2U_m - \Delta x \cdot U_{mx} - \Delta y \cdot U_{my})/8$$
$$- (\Delta t/16)(2F_m - \Delta y \cdot F_{my} + \Delta t \cdot F_{mt}/2)/\Delta x$$
$$- (\Delta t/16)(2G_m - \Delta x \cdot G_{mx} + \Delta t \cdot G_{mt}/2)/\Delta y$$

To proceed, we assume U_m^* from different SEs at the common grid points A, B, C and D have the same values. Refer to Fig. 2(b). And, we have

$$(U_{mx})_{i,j}^n = [(U_{ml_1})_{i,j}^n + (U_{ml_2})_{i,j}^n]/2\cos(\theta) \quad (2.12a)$$
$$(U_{my})_{i,j}^n = [(U_{ml_1})_{i,j}^n - (U_{ml_2})_{i,j}^n]/2\sin(\theta) \quad (2.12b)$$

Here
$$(U_{ml_1})_{i,j}^n = [(U_{ml_1}^+)_{i,j}^n + (U_{ml_1}^-)_{i,j}^n]/2 \quad (2.13a)$$
$$(U_{ml_2})_{i,j}^n = [(U_{ml_2}^+)_{i,j}^n + (U_{ml_2}^-)_{i,j}^n]/2 \quad (2.13b)$$
$$(U_{ml_1}^\pm)_{i,j}^n = \pm[(U_m')_{i\pm1/2, j\pm1/2}^n - (U_m)_{i,j}^n]$$
$$/(\sqrt{\Delta x^2 + \Delta y^2})$$
$$(U_{ml_2}^\pm)_{i,j}^n = \pm[(U_m')_{i\pm1/2, j\mp1/2}^n - (U_m)_{i,j}^n]$$
$$/(\sqrt{\Delta x^2 + \Delta y^2})$$
$$(U_m')_{i\pm1/2, j\pm1/2}^n = \{U_m + \Delta t \cdot U_{mt}/2\}_{i\pm1/2, j\pm1/2}^{n-1/2}$$

And
$$\cos(\theta) = \Delta x/\sqrt{\Delta x^2 + \Delta y^2}$$
$$\sin(\theta) = \Delta y/\sqrt{\Delta x^2 + \Delta y^2}$$

U_{ml1} and U_{ml2} can be considered as two directional derivatives. For the computations of flow problems with discontinuities, Eq. (2.13) can be replaced by the re-weighting function (2.9) or the minmod limiter (2.10). Equations.(2.11) to (2.13) are the modified CE/SE scheme for the two-dimensional Euler equations for the CE and SE of the second kind.

3. Modified CE/SE Scheme for the Two-Dimensional Navier-Stokes Equations

Consider the two-dimensional Navier-Stokes Equations:
$$\partial U_m/\partial t + \partial F_m/\partial x + \partial G_m/\partial y$$
$$- \partial F_{vm}/\partial x - \partial G_{vm}/\partial y = 0, \, m=1,2,3,4 \quad (3.1)$$

where F_v and G_v are the viscose fluxes. The integral counterpart of Eq. (3.1) is

$$\oint_{S(V)} \tilde{H}_m \cdot ds = 0, \quad m=1,2,3,4 \quad (3.2)$$

Where
$$\tilde{H}_m = (F_m - F_{vm}, G_m - G_{vm}, U_m).$$

To proceed, the CE and SE of the first kind is used. Similar to the treatment for the Euler equations, the space-time flux conservation Eq.(2.5) is enforced over a CE. However, the H_m^* includes the viscous terms:
$$\tilde{H}_m^*(x, y, t; i, j, n) = (F_m^*(x, y, t; i, j, n) - F_{vm},$$
$$G_m^*(x, y, t; i, j, n) - G_{vm}, U_m^*(x, y, t; i, j, n)) \quad (3.3)$$

Since the viscose fluxes involve spatial gradient of flow variables, the midpoint rule is used to integrate the viscous fluxes. For example, the integral of F_v on the surface FQQ'F' is calculated by
$$\int_{FQQ'F'} F_v \cdot dS = (\Delta t \cdot \sqrt{(\Delta x)^2 + (\Delta y)^2}/8) \cdot$$
$$F_v((U_m, U_{mx}, U_{my})_{i+3/8, j+1/8}^{n-1/4}) \quad (3.4)$$

Where
$$(U_m)_{i+3/8, j+1/8}^{n-1/4} = (U_m)_{i+1/2, j}^{n-1/2} - (\Delta x/8) \cdot (U_{mx})_{i+1/2, j}^{n-1/2}$$
$$+ (\Delta y/8) \cdot (U_{my})_{i+1/2, j}^{n-1/2} + (\Delta t/4) \cdot (U_{mt})_{i+1/2, j}^{n-1/2}$$
And
$$(U_{mx})_{i+3/8, j+1/8}^{n-1/4} = (U_{mx})_{i+1/2, j}^{n-1/2}$$
$$(U_{my})_{i+3/8, j+1/8}^{n-1/4} = (U_{my})_{i+1/2, j}^{n-1/2}$$

As a result, the discrete equation for U_m is

$$(U_m)_{i,j}^n = \{Q_m^{(2)}(\Delta y/2) - [(\lambda F_v + \eta G_v)_{(x_1, y_1)}^{n-1/4}$$
$$- (-\lambda F_v + \eta G_v)_{(x_2, y_2)}^{n-1/4}\}_{i, j+1/2}^{n-1/2}$$
$$+ \{Q_m^{(2)}(-\Delta y/2) - [(-\lambda F_v - \eta G_v)_{(x_5, y_5)}^{n-1/4}$$
$$- (\lambda F_v - \eta G_v)_{(x_6, y_6)}^{n-1/4}\}_{i, j-1/2}^{n-1/2}$$
$$+ \{Q_m^{(1)}(-\Delta x/2) - [(-\lambda F_v + \eta G_v)_{(x_3, y_3)}^{n-1/4}$$
$$- (-\lambda F_v - \eta G_v)_{(x_4, y_4)}^{n-1/4}\}_{i-1/2, j}^{n-1/2}$$
$$+ \{Q_m^{(1)}(\Delta x/2) - [(\lambda F_v - \eta G_v)_{(x_7, y_7)}^{n-1/4}$$
$$- (\lambda F_v + \eta G_v)_{(x_8, y_8)}^{n-1/4}\}_{i+1/2, j}^{n-1/2}$$
$$(3.5)$$

Here $\lambda = \Delta t/\Delta x$, $\eta = \Delta t/\Delta y$, and $(x_1, y_1, t^{n-1/4})$, $(x_2, y_2, t^{n-1/4})$, ..., $(x_8, y_8, t^{n-1/4})$ are geometric centers of the plans AHH'A', AEE'A',...,DHH'D'.

In addition, it is better to include the viscous effect in the calculation of the time derivative term, for example, we can use:

$$(U_{mt})_{i,j}^n = -(F_{mx})_{i,j}^n - (G_{my})_{i,j}^n$$
$$+ [(F_{vm})_{i+1/2,j}^n - (F_{vm})_{i-1/2,j}^n]/\Delta x$$
$$+ [(G_{vm})_{i,j+1/2}^n - (G_{vm})_{i,j-1/2}^n]/\Delta y$$

(3.6)

Because of Eq. (3.6), we use the dual mesh approach in solving the Navier-Stokes equations. That is, at every time level, flow variables at every grid point are calculated. To U_{mx} and U_{my}, Eqs. (2.8) or (2.9) is used. Equations (3.5), (2.8) or (2.9) are the modified CE/SE method for solving the two-dimensional Navier-Stokes equations. Using the same approach, we can also get a similar scheme corresponding to the second definition of CE and SE. The above schemes can be easily extended to three-dimensional case.

4. Boundary Condition Treatments

In the CE/SE method, the boundary condition treatment is based on space-time flux conservation; it is very simple and can be easily implemented. For Euler equations, two boundary conditions are of concern: the reflective boundary condition and the non-reflective boundary condition. At the outlet or free surface, the non-reflective boundary condition are used. On solid walls or along a symmetry surface, the reflective boundary condition is applied. For the Navier-Stokes equations, the no-slip condition along a wall boundary must be considered. In the setting of the CE/SE method, two treatments for the no-slip condition along wall boundaries are proposed, namely, the traditional solid boundary condition and the pseudo–reflective boundary condition.

4.1 Traditional Wall Boundary Conditions

Along a wall boundary, the non-slip condition is used, i.e., $u_w = v_w = 0$. In addition, the distribution of heat flux q_n along the wall should be provided. Or, wall temperatures T_w should be given. Usually, an additional boundary condition is needed along the wall. The traditional approach is to specify null pressure gradient vertical to the wall along the boundary, i.e., $\partial P/\partial n=0$. This condition is reasonable for boundary layer type flows. However, for flows with separation along the wall boundary, this treatment is only an approximation. To recap, the traditional boundary conditions along an insulated wall are

$$\begin{cases} u_w = 0 \\ v_w = 0 \\ \partial T/\partial n = 0 \\ \partial P/\partial n = 0 \end{cases}$$

(4.1)

4.2 Pseudo-Reflective Boundary Conditions

For a wall parallel to the x-coordinate, no grid point at the solid wall is used. Instead, a reflective point blow the wall is used. This arrangement is similar to the boundary condition for solving the Euler equations. Refer to Fig. 3. To calculate the flow variables at E, we use its mirror image, i.e., point E' below the solid wall. Along the wall, since $u_w = v_w = 0$, the flux normal to the wall is

$$F - F_v = \begin{pmatrix} 0 \\ -\dfrac{\mu}{R_{eL}} \cdot \dfrac{\partial u}{\partial y} \\ P - \dfrac{\mu}{R_{eL}} \cdot \dfrac{\partial v}{\partial y} \\ q_y \end{pmatrix}$$
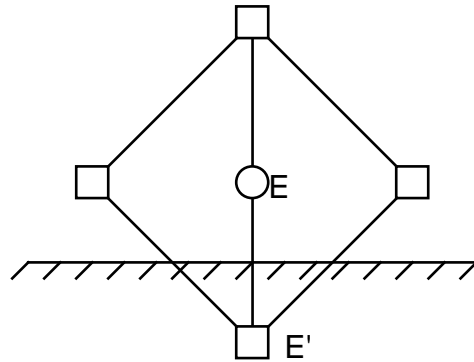
(4.2)

Fig. 3 A schematic of the grid point distribution near the solid boundary

Since when the viscosity μ approaches zero, the Navier Stokes solution should asymptotically approach the solution of the Euler equations. Therefore, the above vertical flux Eq. (4.2) could be further modified by imposing the reflective conditions along the wall. In addition, if the insulated condition is used for the energy equation, one only needs to evaluate the value of $\partial u/\partial y$ in the calculation of the normal flux through the wall.

In this pseudo-reflective wall boundary treatment, no unnecessary assumption is used. Thus it is simpler than the traditional boundary condition and it can be easily to be implemented. For the natural convection case, numerical results obtained using the pseudo-reflective solid wall boundary condition treatment are better than that obtained by the traditional one.

5. Numerical Results

In order to test the robustness and efficiency of the present schemes, several prototype flow problems are calculated.

5.1 Shock Diffraction Around a 90° Corner

This example is a test for the Euler solver based on the modified CE/SE method. At $t=0$, the calculation is initiated with a shock located at the corner. Reflective boundary condition is applied on the upper and lower surfaces and on all walls. The computational domain is 4.7×3.6 and Mach number is $M_s = 2.4$. A uniform mesh of 110×45 is used. Figure 4 shows the density contours at three different times. The result agrees well with the experimental result [5].
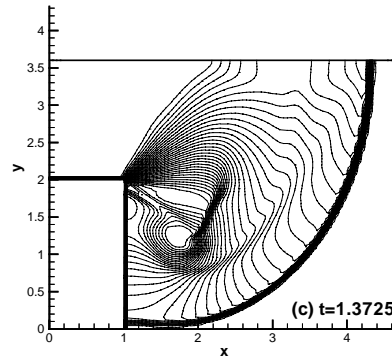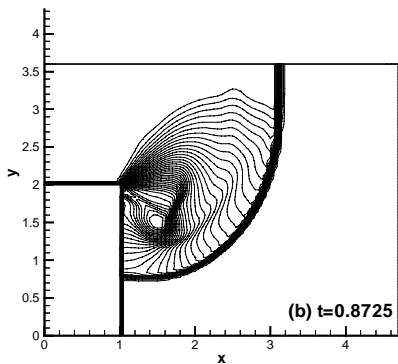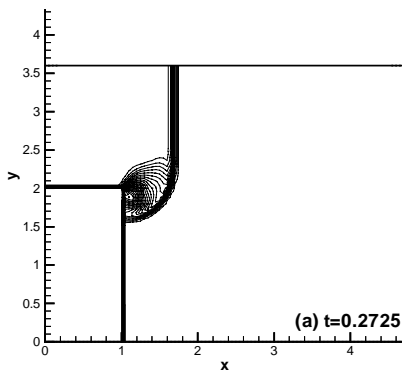

Fig.4 Density contours for shock wave diffraction around a 90° corner

5.2 Blast Wave Problem

In this case, a blast wave generated by an open ended cylindrical shock tube is simulated. This problem is solved using the Euler solver. The shock tube configuration and the initial conditions are set up according to [5]. Initially, the compressed gas inside the tube is separated from the surrounding stagnant gas by a diaphragm located at the outlet of the tube. At $t=0$, the calculation is initiated by a sudden removal of the diaphragm. The direct contact of the high and low pressure regions results in a rarefaction wave propagating back into the tube and a shock wave blasting from the tube lip into the ambient space. A uniform mesh of 80×60 is used. The non-reflective boundary condition is used at the inlet and outlet of the computational domain, while the reflective boundary condition is used on the symmetric axis and the tube walls. Figure 5 shows flow solutions at two different times. The results agree well with the experimental results[5].
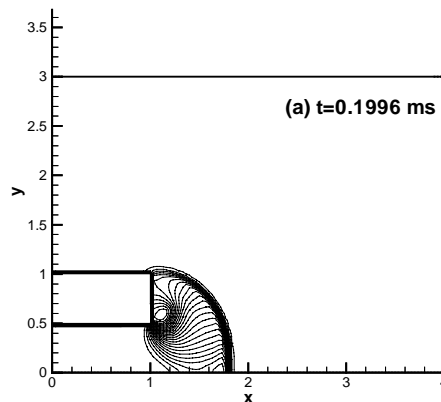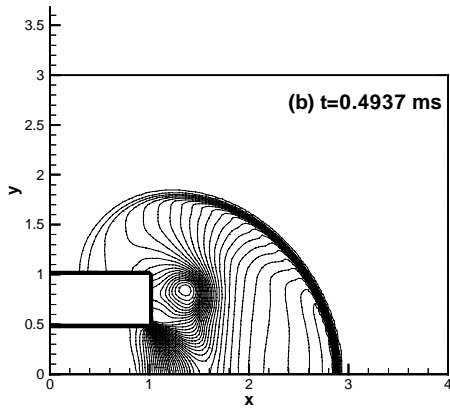
Fig.5 Pressure contours for blast wave problem

5.3 Shock/ Boundary Layer Interactions

Because of its simple geometry, shock/boundary layer interaction is a standard test problem for various Navier Stokes solvers. But the flow pattern of this problem are very complicated. When the shock is strong enough, boundary layer separation occurs at the shock impinging point. In order to resolve the boundary layer, clustered grid points near the solid wall must be employed. Here a simple coordinate transformation is used:

$$\begin{cases} \sigma = x \\ \tau = \log[1 + y(e^K - 1)/H]/K \end{cases} \qquad (5.1)$$

where K is a stretching parameter and H is the height of the physical domain. Larger K implies more grid points clustered near the wall.
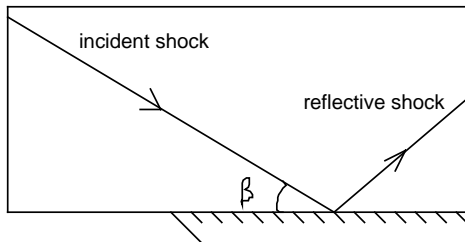
Fig.6 A schematic of the shock/boundary layer interaction.

In this problem, the free-stream Mach number is $M_\infty = 2.0$. The Reynolds number is $R_e = 2.96 \times 10^5$. The shock incident angle $\beta = 32.6^o$.

The computational domain is $[0, 0.12] \times [0, 0.06]$. A 180×160 non-uniform mesh is used.
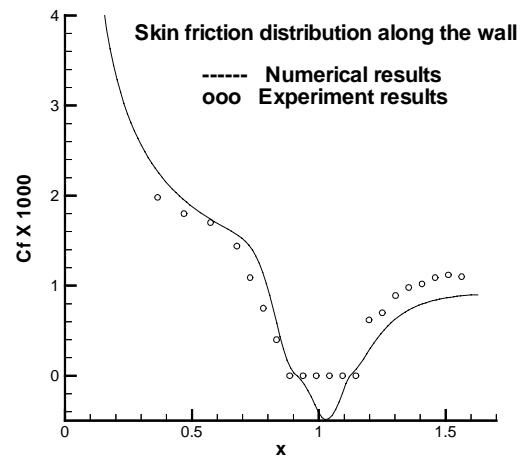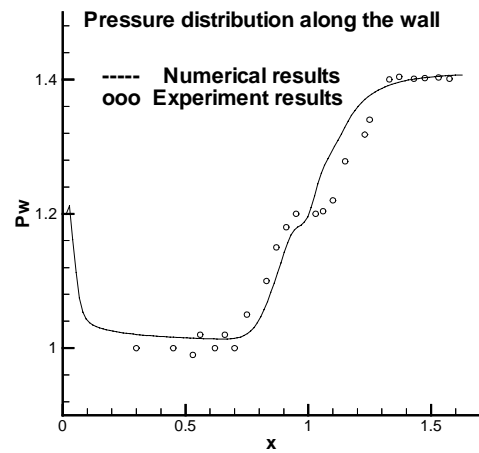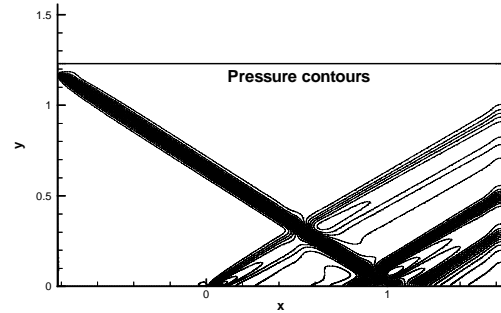

Fig.7 Numerical results of shock/boundary layer interaction using the traditional wall boundary condition: (a) pressure contours, (b) pressure distribution along the wall, and (c) skin friction distribution along the wall

In this case, two different wall boundary conditions are used. The numerical results are shown in Fig.7 and Fig.8, for pressure contours, pressure distribution along the wall, and skin friction distribution along the wall. The differences between these two solid wall boundary treatments are very small, but they all agree well with the experiment results[18].
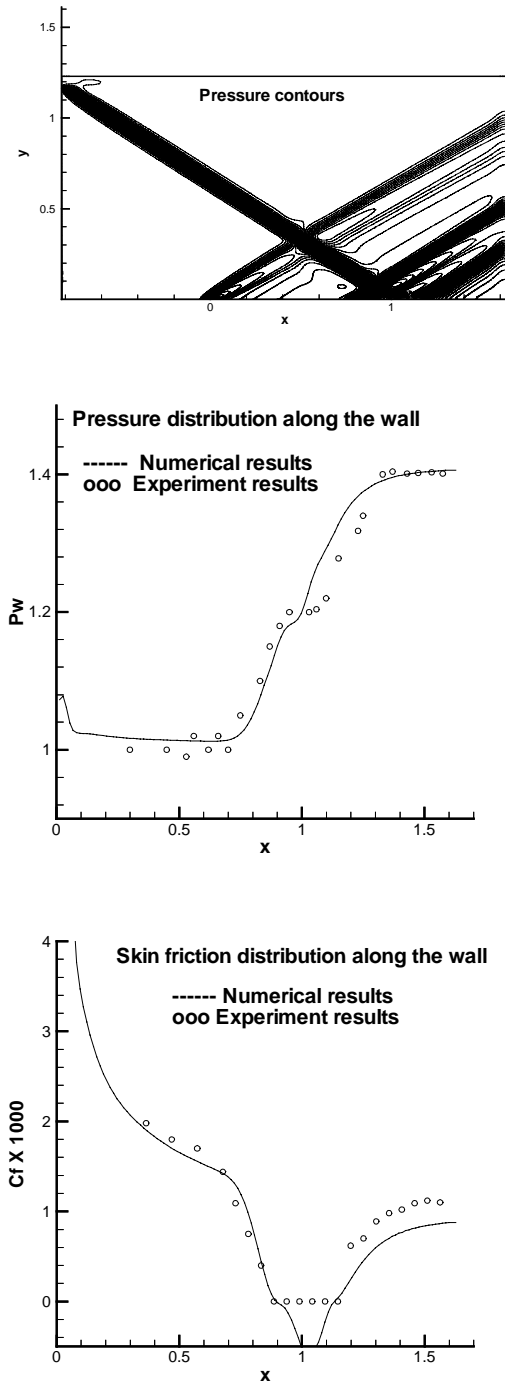

Fig.8 Numerical results of shock/boundary layer interaction using the pseudo-reflective boundary condition: (a) pressure contours (b) pressure distribution along the wall and (c) skin friction distribution along the wall.

5.4 Natural Convection Flows in a Square Box

The last numerical example is a buoyancy-driven gas flow in a square enclosure. As shown in Fig.9, the configuration consists of two insulated horizontal walls and two lateral walls with constant temperatures of T_h and T_c. For a small temperature difference between two vertical walls, this problem has been extensively studied based on the incompressible flow equations with Boussinesq model for the buoyancy force. For a large temperature difference, the compressible formulation should be employed.
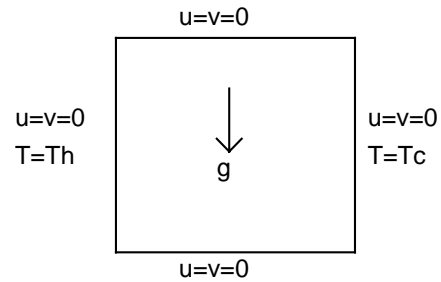

Fig.9 A schematic of the buoyancy-driven gas flow in a box

Flow features of this buoyancy-driven cavity flow depend on Raylaigh number R_a, Frounde number F_r, the aspect ratio of the cavity, and the temperature difference parameter ε. Here, four Raylaigh numbers $R_a =10^3$, 10^4, 10^5 and 10^6 are considered with a temperature difference parameter $\varepsilon = 0.6$, which represents $T_h/T_c =4$. The Frounde number and the aspect ratio are unity. This problem is calculated using the modified scheme, i.e., Eqs. (3.5) and (2.8) with a uniform mesh 120×120. The pseudo-reflective boundary treatment is used. Figure 10 shows the velocity vectors at four Raylaigh numbers. Figures11 and 12 are the x and y-direction velocity distributions along the vertical and horizontal centerlines at Ra = 10^4. The solution by the CE/SE method agrees well with previously reported data [19].
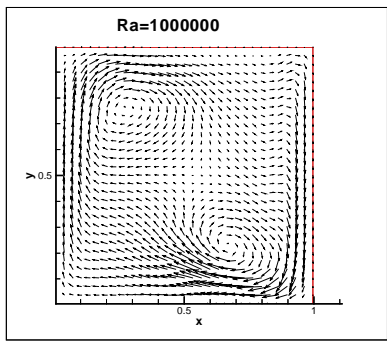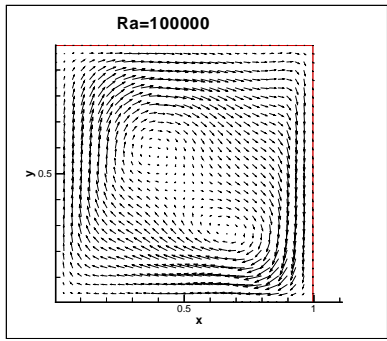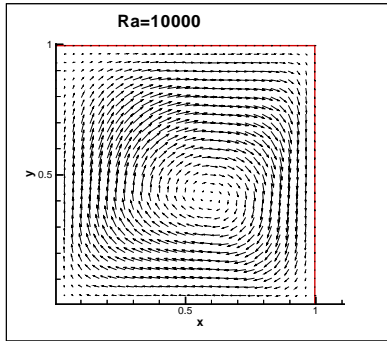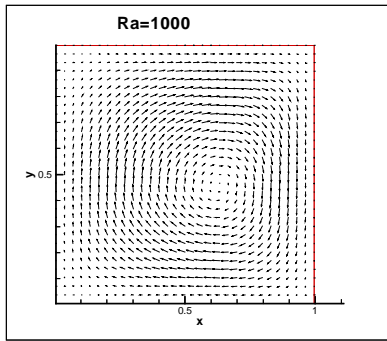
Fig.10 Velocity vectors of the buoyancy-driven flow
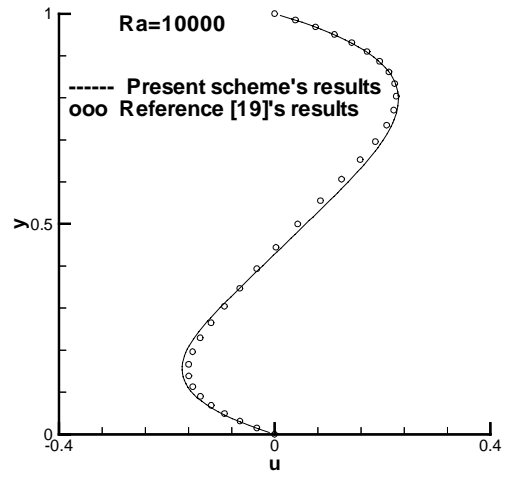at four Raylaigh numbers

Fig.11 Velocity u distribution along the vertical
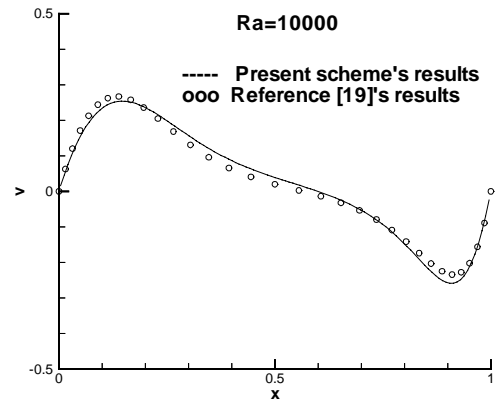centerline

Fig.12 Velocity v distribution along the horizontal
centerline

Concluding Remarks

In this paper, we report a modified space-time CE/SE method for Euler and Navier Stokes equations for structured meshes. Because of the use of simpler CE and SE, the logic of the modified CE/SE method is simpler and thus the computation is more efficient. Nevertheless, the modified space-time CE/SE schemes retain all favorable features of the original CE/SE method, including the unified treatment of space and time, accurate computation of space-time flux conservation, and high-fidelity resolution of unsteady flow field.

In the Navier-Stokes solver, the calculation of the viscous fluxes is based on a mid-point rule, which is simple and effective. Because the calculation of the viscous fluxes involves the calculation of first order derivatives, the duel mesh operation is used. In addition two wall boundary conditions, i.e., the traditional one and the pseudo-reflective one, are used. The latter is simpler and more robust. Moreover, the Navier Stokes solver of the CE/SE scheme can be applied to high speed flows as well as low-Mach-number flows without preconditioning.

Numerical results of several standard flow problems show that the numerical accuracy of the modified CE/SE schemes is comparable to the original CE/SE method. All numerical results reported in this paper agree well with the experimental or previously reported numerical results.

References

1. Chang, S.C., "The Method of Space-Time Conservation Element and Solution Element – A New Approach for Solving the Navier Stokes and Euler Equations," *J. Comp. Phys.*, Vol. 119 , 1995, pp. 295-324

2. Chang, S.C., Yu, S.T., Himansu, A., Wang, X.Y., Chow, C.Y. and Loh, C.Y., "The Method of Space-Time Conservation Element and Solution Element – A New Paradigm for Numerical Solution of Conservation Laws," *Computational Fluid Dynamics Review*, Vol.1, 1998, pp. 206-240. Editors: Hafez, M. and Oshima, K., World Scientific Publisher.

3. Chang, S.C. and Himansu, A., "The Implicit and Explicit a-μ Schemes," NASA/TM 97-206307, 1997.

4. Chang, S.C., Himansu, A., Loh, C.Y., Wang, X.Y., Yu S.T., Jorgenson, P., "Robust and Simple Nonreflecting Boundary Conditions for the Space-Time Conservation Element and Solution Element Method," AIAA Paper 97-2077, the 13th AIAA CFD Conference, June 1997, Snow Mass, CO.

5. Wang, X.Y., "Computational Fluid Dynamics based on the Method of Space-Time Conservation Element and Solution Element," Ph.D. Dissertation, Univ. of Colorado at Boulder, 1995.

6. Zhang, Z.C., "A Modified Space-Time Conservation Element and Solution Element Schemes," Report at the Beijing Workshop on CFD (8) (in Chinese), 1996.10, pp. 50-54.

7. Zhang, Z.C., Shen, M.Y., "New Approach to Obtain Space-Time conservation Schemes," *Chinese J. of Aeronautics*, 1997, 10(2), pp. 87-90

8. Zhang, Z.C., Shen, M.Y., "Improved Scheme of Space-Time Conservation Element and Solution Element," *J. of Tsinghua University (Sci & Tech)*, (in Chinese), 1997, 37(8), pp. 65-68.

9. Zhang, Z.C., "Modified Space-Time Method for Solving Conservation Laws," *Chinese J. of Computational Mechanics* (in Chinese), 1997, 14 (special issue), pp. 741-744

10. Zhang, Z.C., "A New General Space-Time Conservation Scheme for 2D Euler Equations," *Chinese J. of Computational Mechanics* (in Chinese), 1997, 14(3), pp. 377-381

14 Zhang, Z.C., Shen, M.Y. and Li, H.D., "Modified Space-Time Conservation Schemes for 2D Euler Equations," 7th Inter. Symposium on CFD, 1997.9, Beijing, China, pp. 253-258.

15 Zhang, Z.C., Li, H.D. and Shen, M.Y., "Sapce-Time Conservation Scheme for 3D Euler Equations," 7th Inter. Symposium on CFD, 1997.9, Beijing, China, pp. 259-262.

16 Zhang, Z.C. and Shen, M.Y., "Modified Space-Time Conservation Scheme for Solving Conservation Laws with Stiff Source Terms," Proceedings of ICFM-III, Beijing, China, 1998.7, pp. 821-826.

17 Zhang, Z.C. and Yu, S.T., "Shock Capturing without Riemann Solver---A Modified Space-Time CE/SE Method for Conservation Laws," AIAA Paper 99-0904, Jan. 1999.

18 Hakkinen, R.J., Greber, I., Trilling, L. and Abarbanel, S.S., "The Interaction of an Oblique Shock Wave with a Laminar Boundary Layer," NASA Memo 2-18-59W, 1959.

19 Yu, S.T., Jian, B.N., Wu, J. and Liu, N.S., "A div-curl-grad formulation for compressible buoyant flows solved by the least-squares finite element method," *Comput. Methods Appl. Mech. Engrg.,* 1996, Vol.137, pp. 59-88